Disorder and thermal transport in undoped $KTaO_3$

1994 J. Phys.: Condens. Matter 6 4077

(http://iopscience.iop.org/0953-8984/6/22/007)

J. Phys.: Condens. Matter 6 (1994) 4077–4092. Printed in the UK

Disorder and thermal transport in undoped $KTaO_3$

B Salce†, J L Gravil† and L A Boatner‡

† CEA, Département de Recherche Fondamentale sur la Matière Condensée, SPSMS/LCP, 38054 Grenoble Cédex 9, France

‡ Solid State Division, Oak Ridge National Laboratory, Oak Ridge, TN 37830, USA

Received 27 September 1993, in final form 3 February 1994

Abstract. The thermal conductivity of nominally pure $KTaO_3$ exhibits an unexpected strong phonon scattering around 8 K. The question arises whether this scattering is related to the distorted microregions observed by other experiments. We have investigated a set of undoped single crystals grown by different methods. By comparison with doped specimens, it is suggested that acoustic phonons are coupled to the soft optic mode via the local disorder. From complementary dielectric permittivity and electron paramagnetic resonance experiments, oxygen vacancies and rhombic Fe^{3+} appear to be incontestable candidates to account for the distorted microregions.

1. Introduction

For a long time, perovskite ABO_3 type potassium tantalate has been known as an incipient ferroelectric. Decreasing temperature results in the softening of the TO_1 transverse optic zone centre phonon branch, but, as the soft mode is stabilized by zero-point quantum fluctuations, $KTaO_3$ does not undergo a ferroelectric transition and remains in the high-temperature paraelectric cubic phase down to 0 K. Owing to the unusually high polarizability, various types of ordered phases can be induced by replacing the Ta or K ions by impurities (Nb, Na, Li). The mixed crystals are thus of great interest regarding the microscopic origins of phase transitions and the role of high-temperature precursor effects [1–4].

Concerning the nominally pure $KTaO_3$, several experiments show anomalous behaviour. The most important information has been gained via optical measurements: first-order lines, forbidden in the perfect perovskite structure, appear in Raman spectra. This result points to the existence of symmetry-breaking defects (SBD) inducing local disorder [5, 6]. The origin of the disorder still remains a matter of controversy: both intrinsic off-centre Ta displacements and extrinsic unavoidable impurities have been invoked [7–9].

Thermal conductivity $K(T)$ measurements show another striking effect: a strong phonon scattering appears at $T < 30$ K, which is sample-dependent. In some cases, a true minimum is evidenced around 8 K, but below 1 K no extra scattering is observed except for the well known boundary diffusion. This behaviour was tentatively explained by invoking a direct 'soft mode–acoustic phonon' interaction, as the decrease in $K(T)$ is enhanced and shifted to lower temperature in Nb-doped $KTaO_3$ (KTN) [10–13].

Some years ago, Lawless investigated the specific heat $C_p(T)$ of both nominally pure and Nb-doped $KTaO_3$ single crystals in the temperature range 2 to 20 K [14, 15]. Surprisingly, the undoped sample exhibited a higher specific heat than KTN. Moreover, the $T \rightarrow 0$ extrapolated $C_p(T)$ value disagreed with the expected Debye limit (calculated by using the measured elastic constants), but no explanation was suggested to account for these results.

0953-8984/94/224077+16$19.50

In order to understand these discrepancies and to start studying the mixed crystals with a well defined reference material, questions about high-quality undoped $KTaO_3$ must be addressed.

It is the purpose of the present paper to check this point carefully by investigating insulating samples provided by several laboratories and grown by different methods (section 2). The investigations were performed by measuring thermal conductivity and complex dielectric permittivity, and the results compared with optical data (section 3). In section 4 indications about the microscopic origin of the disorder are proposed with the aid of electronic paramagnetic resonance (EPR) measurements. Finally, section 5 will be devoted to data relative to what we presume to be the 'purest' now available $KTaO_3$ single crystals.

2. Samples and techniques

$KTaO_3$ crystallizes in the ABO_3 perovskite structure with Ta^{5+} at the centre of the oxygen octahedra. The soft TO_1 mode can be represented as the vibration of the rigid oxygen cage against Ta ions along a ⟨100⟩ axis. Two different methods have been mainly used to grow $KTaO_3$ crystals of large size and high perfection: 'top-seeded solution growth' (TSSG) and 'spontaneous nucleation' (SN) within a slowly cooled flux [16]. The latter can be modified to grow blue semiconducting and colourless pure material coexisting in the same crystal (SN/M). In the following, we report measurements performed on the samples listed in table 1. Besides the undoped specimens, a number of samples with small concentrations of various doping ions have been investigated in order to highlight the physical properties.

Concerning the pure samples, most of them were grown by one of us (LAB) at the Oak Ridge National Laboratory (ORNL). They can be classified into two different groups, respectively labelled P and UP. From a historical point of view, the P samples are the oldest and grown by the SN method. UP crystals are grown more recently by the SN/M technique. Sample R (SN) was loaned by D Rytz (Sandoz Produkte Cie), and Professor S Jandl (University of Sherbrooke) provided us with specimen J (TSSG). Doped samples were grown at the ORNL by the SN method, except the sample labelled Nb–(U), which was provided by H Uwe (University of Tsukuba).

The thermal conductivity data were obtained by the use of the classical steady-state method from room temperature down to 50 mK. In some cases, a bias electric field up to 15 kV cm^{-1} was applied to the sample. Gold electrodes (500 Å thick) were vacuum deposited onto opposite faces of samples in order to measure the complex dielectric permittivity $\epsilon = \epsilon' + i\epsilon''$. The values of ϵ' and ϵ'' were recorded by using a computer-controlled General Radio 1689 capacitance bridge (frequencies 12 Hz–100 kHz). The measuring field ranged from 36 (UP–(2)) to 250 V cm^{-1} (UP–(3)). Measurements were performed in a dynamic way that allowed cycling at the rate of $\simeq 1$ K min^{-1} from 300 to 2 K. EPR experiments were performed at room temperature in a Varian 109 spectrometer operating at $\simeq 9$ GHz.

3. Experimental results

3.1. Thermal conductivity

Some of these results have been reported previously [11–13]. A comprehensive paper concerning thermal transport in both nominally pure and doped $KTaO_3$-based materials will

Table 1. Sample characteristics.

Sample[a]	Doping	Growth method	dimensions (mm^3)
UP–(a)†	Und.[b]	SN/M	**5.47** × 2.37 × *0.48*
UP–(b)†	Und.	SN/M	**5.47** × 2.15 × *1.03*
UP–(1)‡	Und.	SN/M	**9.50** × 3.45 × *2.58*
UP–(2)‡	Und.	SN/M	**25.70** × 4.80 × *2.80*
UP–(3)‡	Und.	SN/M	**13.20** × 4.60 × *0.40*
P–(B)	Und.	SN	**6.39** × 2.36 × *1.68*
P–(G)	Und.	SN	**9.22** × 2.86 × *0.60*
P–(S)	Und.	SN	**7.44** × 2.77 × *0.60*
P–(88)	Und.	SN	**11.93** × 3.31 × *0.44*
P–(R)	Und.	SN	**3.78** × 3.53 × *2.74*
P–(J)	Und.	TSSG	**11.00** × 3.15 × *2.08*
Nb–(B1)	0.15% Nb	SN	**13.30** × 2.78 × *2.06*
Nb–(B2)	0.80% Nb	SN	**8.34** × 2.46 × *2.16*
Nb–(U)	>0.1% Nb	SN	**3.00** × 3.00 × *0.47*
Na–(B)	1% Na	SN	**14.22** × 2.20 × *1.62*
Li–(B)	1.5% Li	SN	**14.72** × 2.76 × *2.74*
Fe–(B1)§	1% Fe	SN	**10.73** × 2.07 × *1.88*
Fe–(B2)§	1% Fe	SN	**10.52** × 1.83 × *1.74*

[a] Identical symbols (†, ‡, §) indicate samples from the same batch. The heat flux was along the **bold** dimension. Electrodes were deposited on opposite faces perpendicular to the *italic* dimension.
[b] Undoped.

be published in the near future. We present only those features of $K(T)$ which are of importance in our discussion. They are compared with the behaviour of what is called a 'nearly perfect insulating crystal' (NPIC), like crystalline quartz or aluminium oxide Al_2O_3 [17, 18].

3.1.1. Nominally pure $KTaO_3$.

Qualitative observations. Figure 1 shows the thermal conductivity of four representative samples, on a logarithmic scale, between 50 mK and 300 K. It is seen that $K(T)$ depends strongly on the specimen. In order to examine these data in a more explicit way, we split the whole temperature range into three different regions.

(i) High temperatures ($T > 50$ K). As T increases, the experimental curves merge and the conductivity becomes sample-independent. This means that $K(T)$ is governed by intrinsic phonon–phonon scattering due to the anharmonic nature of the lattice forces. This mechanism is commonly observed in NPIC.

(ii) Low temperatures ($T < 1$ K). The slopes of the different curves tend to a T^3 dependence. In dielectric compounds, this behaviour is associated with the limitation of the phonon mean free path by crystal boundaries (Casimir regime). Then, the magnitude of $K(T)$ depends on the size of the specimen and on the roughness of surfaces. As an example, samples UP–(a) and UP–(b) have been cut from the same ingot: it is observed that the measured conductivities are quite similar above 5 K, but exhibit a ratio of 2 at the lowest temperatures, reflecting the difference in their cross section (see table 1). Our set of

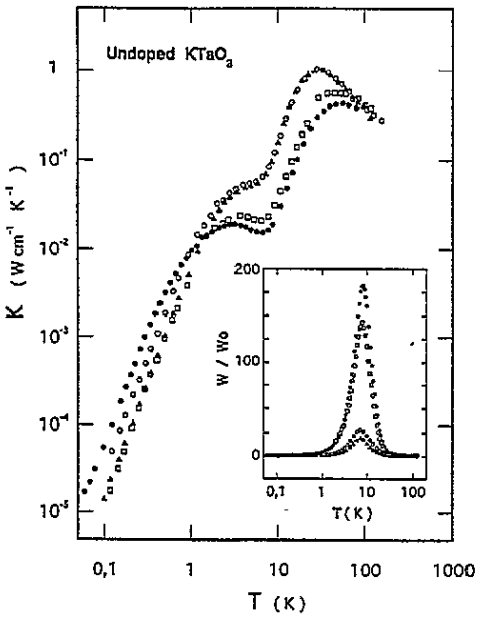

Figure 1. The thermal conductivity of four undoped samples of $KTaO_3$: (●) P–(B), (▲) UP–(a), (○) UP–(b), (□) P–(R). Insert: the reduced thermal conductivity W/W_0.

data is consistent with the dimensions of the samples under investigation, leading us to the conclusion that no additional scattering appears below 1 K.

(iii) Intermediate temperatures (1 K $< T <$ 50 K). In the case of NPIC, $K(T)$ is dominated by dislocation and point-defect scattering. These processes are always present in a real crystal and are considered as 'intrinsic'. They give rise to a monotonic, smooth variation up to a maximum achieved when phonon–phonon scattering becomes dominant.

Whatever the origin of the specimens, the thermal conductivity of undoped $KTaO_3$ exhibits strong 'additional' phonon scattering. Depending on the sample, a change of slope or a true minimum around T_m(und.) $\simeq$ 8 K is observed: it was conjectured that the absence of a minimum should be due to the better quality of the UP samples. However, new experiments carried out on large-sized UP crystals have shown the existence of a true minimum (see figure 3). It is now well established that the absence of a minimum occurs in thin samples (< 1 mm). In this case, the boundary scattering is large enough to be the dominant mechanism in limiting the phonon mean free path up to 5–10 K, preventing the observation of the minimum.

The 'additional' phonon scattering. To emphasize more clearly the 'additional' phonon scattering, we have plotted the data in the form W/W_0, where $W = 1/K(T)$, and $W_0 = 1/K_0(T)$ is the thermal resistivity calculated by taking into account the intrinsic scattering only. This can be done in a straightforward manner by using the Debye approximation and the relaxation time model. The thermal conductivity is given by the classical integral [18]:

$$K(T) = \frac{k_B}{2\pi^2 v}\left(\frac{k_B T}{\hbar}\right)^3 \int_0^{\Theta_D/T} \frac{x^4 e^x}{(e^x-1)^2}\frac{1}{\tau^{-1}(\omega, T)}\,dx$$

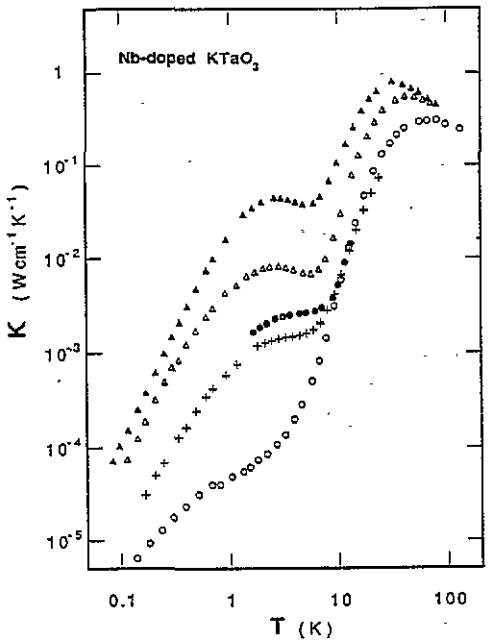

Figure 2. The thermal conductivity of three Nb-doped $KTaO_3$: (△) Nb–(B1), (○) Nb–(B2) with $E = 0$, (●) Nb–(B2) with $E = 15$ kV cm^{-1}, (+) Nb–(U); together with the data for an undoped specimen: (▲) UP–(2).

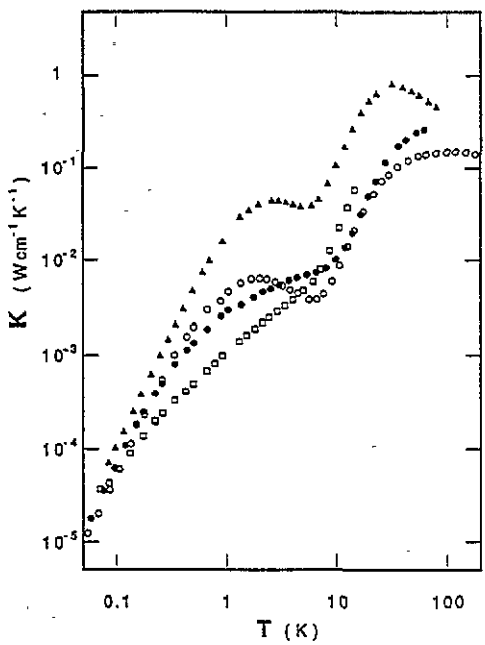

Figure 3. comparison between the thermal conductivity of $KTaO_3$ specimens with various doping: (○) Na–(B), (●) Li–(B), (□) Fe–(B1); together with the data for one undoped specimen: (▲) UP–(2).

where $x = \hbar\omega/k_B T$, $\Theta_D = 326$ K is the Debye temperature and $v = 4360$ m s^{-1} is the mean sound velocity. Finally $\tau(\omega, T)$ is the combined relaxation rate obtained by adding the reciprocal relaxation times of the mechanisms involved:

$$\tau^{-1}(\omega, T) = \tau_U^{-1} + \tau_B^{-1} + \tau_D^{-1} + \tau_P^{-1}.$$

In this expression, the following are used: $\tau_U^{-1} = 4.6 \times 10^{-5} \omega T \exp(-\Theta_D/3T)$ describes the phonon–phonon interactions and was taken the same for all samples; $\tau_B^{-1} = v/Lc$ is the relaxation rate for scattering by boundaries—Lc is determined by the sample dimensions and can be adjusted slightly; $\tau_D^{-1} = G\omega$ and $\tau_P^{-1} = A\omega^4$, respectively, accounts for dislocation and point-defect scattering—as they are efficient in the temperature range of the 'additional' scattering, it is difficult to give then precise values. In view of the high crystallographic quality of the specimens, it seems reasonable to use, for the latter, comparable magnitudes as observed in other insulating crystals. So, we get $G = 4 \times 10^6$ and $A = 7 \times 10^{44}$ s^3 for all samples. In fact, changing G or A by a factor of 10 does not affect in a qualitative way the shape of the calculated conductivity. Thus we are able to define a 'reference' thermal resistivity W_0 for each sample.

The reduced thermal resistivity W/W_0 for the same four undoped samples is plotted in figure 1 (insert). A unique maximum occurs around T_m(und.) $\simeq 8$ K for each sample. The scattering vanishes below 1 K but remains efficient up to 30 K. Three features are of particular note, which lead to important remarks:

(i) The shapes of the curves exhibit a pronounced similarity, which clearly emphasizes that the scattering originates from a common mechanism.

(ii) The height of the maximum I_{ph} is sample-dependent, suggesting that the scattering might be due to an extrinsic defect with a concentration that differs from sample to sample.

(iii) The temperature of the maximum is roughly the same for the studied samples, T_m(und.) $\simeq$ 8 K. In the steady-state method, phonons are thermally excited with a black-body distribution. This gives rise to a heat current spectrum with a maximum at a frequency ω_m such as $\hbar\omega_m \simeq 3.8 \times k_B T_m$ ($\hbar\omega_m = 80 \times T$ GHz $= 2.6 \times T$ cm^{-1}). From what is called the 'dominant phonon approximation' [19], a maximum in thermal resistivity at temperature T_m(und.) means that the energy of the most strongly scattered phonons is $\hbar\omega_m = 3.8 \times k_B T_m$(und.), i.e. 18–20 cm^{-1} in the case of undoped $KTaO_3$. This value favourably compares with the low-temperature soft-mode energy $\omega_{TO}(T)$, as deduced from Raman [20] and neutron scattering experiments [21].

From this last remark, it follows that the 'additional' phonon scattering should be a signature of a coupling between the acoustic phonons and the soft optic mode. However, remark (ii) suggests that the coupling could be mediated by impurities or defects.

In order to check this assignment more precisely, we have studied $KTaO_3$ single crystals intentionally doped with various impurities.

3.1.2. Doped crystals. Impurities can be roughly classified into two types.

Non-polar impurities. Elements like Ag, Ni, Co, Cu, Fe, etc., act as point defects and the induced perturbations do not extend over long distances, so that, at a first level, the soft-mode energy is not affected.

Previous measurements done on doped single crystals (with impurity concentrations up to a few per cent) have shown that no significant changes, either in shape or in magnitude, can be observed in the 'additional' phonon scattering [11]. As an exception, Fe-doped $KTaO_3$ exhibited an enhanced scattering at low temperature, although T_m(Fe) was not drastically different from T_m(und.).

Polar impurities. Niobium, sodium and lithium are known to change the soft-mode energy: introducing Nb or Na decreases $\omega_{TO}(T)$ [2,3,22–24], but in contrast replacing K ions by Li results in an increase in $\omega_{TO}(T)$ [25,26]. On the other hand, it has been observed that this frequency is shifted up when a static electric field is applied: near 0 K, this effect is large (factor of 2 with 15 kV cm^{-1}) but disappears above 40 K [27].

$K(T)$ measurements performed on several Nb-doped $KTaO_3$ samples displayed a very strong low-temperature phonon scattering (figure 2), irrespective of the origin of the specimens: Nb–(U) supplied by Professor Uwe looks very similar to crystals grown at the ORNL. Plotted in the form W/W_0, the data show that T_m(Nb) shifts towards 0 K as the niobium concentration increases. Moreover, applying a static electric field ($E_{max} \simeq$ 15 kV cm^{-1}) raises the conductivity and leads to T_m(Nb, $E \neq 0$) > T_m(Nb, $E = 0$) (similar effects are observed on undoped $KTaO_3$ resulting in T_m(und., $E \neq 0$) > T_m(und., $E = 0$)).

Thermal conductivity curves from Na-doped crystals exhibit a sharp minimum around T_m(Na) that is roughly equal to T_m(und.). Samples including lithium are characterized by a special low-temperature ($T < 1$ K) phonon scattering as the observed $K(T)$ obeys a $\sim T^2$ rather than $\sim T^3$ variation and the deduced values T_m(Li) are higher than T_m(und.) (figure 3).

From this set of data, it can be seen that the T_m variations observed in doped crystals are tightly connected with the low-temperature changes in the soft-mode frequency $\omega_{TO}(T)$. The lack of significant change in T_m(Na) can be understood keeping in mind the small amount of sodium ($\simeq$ 1%) in the involved samples relative to the critical concentration of

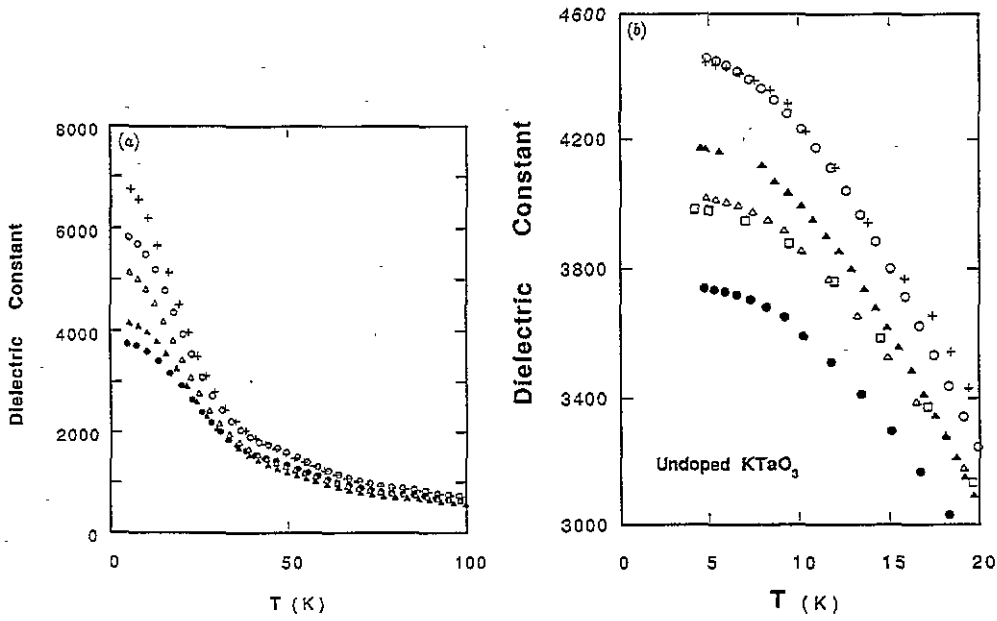

Figure 4. (*a*) Dielectric constant ϵ' (f_m = 1 kHz) for various $KTaO_3$-based specimens: (●) P–(B), (▲) UP–(a), (△) Nb–(B1), (+) Nb–(U), (○) Na–(B). (*b*) Low-temperature part of the dielectric constant of six nominally 'pure' samples of $KTaO_3$: (●) P–(B), (△) P–(S), (+) P–(G), (□) P–(J), (○) UP–(1), (▲) UP–(a).

12%, so that Na merely acts as a point defect, increasing the magnitude of the scattering rather than changing the soft-mode frequency.

These results stressed the idea that the 'additional' phonon scattering in undoped $KTaO_3$ crystals results from the coupling between acoustic and optic phonon branches, and suggested that polar impurities could play a major role in the involved mechanism. In this case, it was expected that dielectric measurements should give additional information and correlate with the magnitude of the phonon scattering I_{ph}.

3.2. Dielectric susceptibilities

Previous data reported for nominally pure $KTaO_3$ samples showed that the real part of the complex dielectric permittivity $\epsilon = \epsilon' + i\epsilon''$ increases as the temperature was lowered, following a Curie–Weiss Law down to $\simeq$ 30 K. Below this temperature, a discrepancy from this behaviour appeared, leading to a flattening below 5 K, but the limiting value ϵ'_{LT} was shown to be sample-dependent and very sensitive to the presence of Nb, Na or Li [28, 29]. Then, we looked for a link between ϵ'_{LT} and I_{ph} to try to get more insight about the nature of the impurities invoked in the previous section (additional details are given by Gravil [30]).

3.2.1. Dielectric constant. Figure 4(*a*) shows ϵ' for several undoped $KTaO_3$ from 100 K down to 4 K at the frequency f_m = 1 kHz. Above 40 K, the data do not significantly depend on the sample. As T is lowered, $\epsilon'(T)$ rises monotonically in the same way as observed in previous studies. At $T < 10$ K, the dielectric constant tends to flatten and reach an upper limit ϵ'_{LT}. As T decreases, the saturation values differ from sample to sample, ranging from 3800 to 4500, which is a roughly 20% spread. Including Nb raises the ϵ'_{LT} value in the expected way.

Surprisingly, no direct relation was established between ϵ'_{LT} and I_{ph}: if ϵ'_{LT}(P–(G))> ϵ'_{LT}(UP–(a)) compares favourably with I_{ph}(P–(G))> I_{ph}(UP–(a)), we observe that ϵ'_{LT}(UP–(a)) is significantly larger than ϵ'_{LT}(P–(B)) (figure 4(*b*)). This result rules out the idea that very low concentrations of polar impurities could be at the origin of the phonon scattering in pure $KTaO_3$: if this assignment was correct, ϵ'_{LT} should be proportional to the defect concentration and ϵ'_{LT}(UP–(a)) should appear as the lowest measured saturation value.

3.2.2. Dielectric losses. As during the runs we simultaneously recorded ϵ' and ϵ'', we have plotted $\tan\delta = f(T)$ (with $\delta = \epsilon''/\epsilon'$) and it was observed that a loss factor peak occurred around $T_L \simeq 40$ K at measuring frequencies f_m in the range 100 Hz–1 kHz (all the samples under study exhibit a detectable peak), which cannot be related in a simple way to a macroscopic structural change of the $KTaO_3$ lattice.

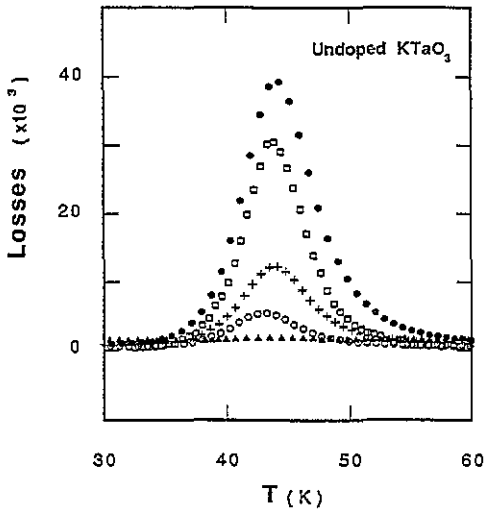

Figure 5. Dielectric losses around 40 K ($f_m = 1$ kHz) of five undoped samples of $KTaO_3$: (●) P–(B), (□) P–(R), (+) P–(G), (○) UP–(1), (▲) UP–(a).

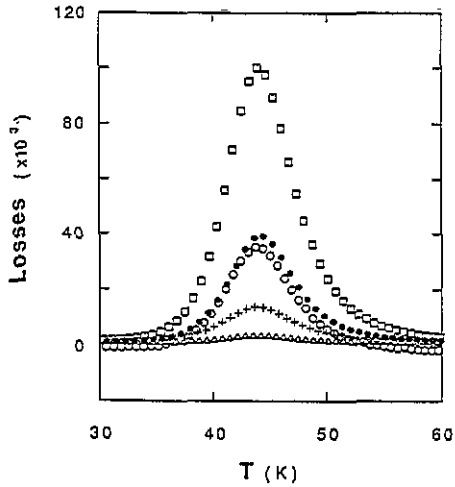

Figure 6. Dielectric losses around 40 K ($f_m = 1$ kHz) of several samples of $KTaO_3$ doped with niobium: (△) Nb–(B1), (+) Nb–(U); sodium: (○) Na–(B); and iron: (□) Fe–(B1); together with the data for an undoped specimen: (●) P–(B).

Examples are given in figure 5. The intensity I_L of the loss peak appears to be strongly sample-dependent and more pronounced in the P specimens, by contrast with the UP samples, which exhibit losses one order of magnitude lower. A similar loss peak was observed in samples doped with polar impurities (figure 6). In figure 7, we have plotted the phonon scattering intensity, roughly given by I_{ph} against I_L for several undoped $KTaO_3$ (a more precise investigation must describe the phonon scattering by using a suitable relaxation time). A reasonable correlation was found, strongly suggesting that the loss factor and the phonon scattering around 8 K could have the same physical origin (we note that one undoped sample does not fit within this law, namely P–(J), which indeed is the only specimen exhibiting several loss peaks between 30 and 50 K, suggesting a complex chemical composition). In the cases of samples doped with polar impurities, I_L depends on the sample but the intensity cannot be related with the doping ion concentration (in some

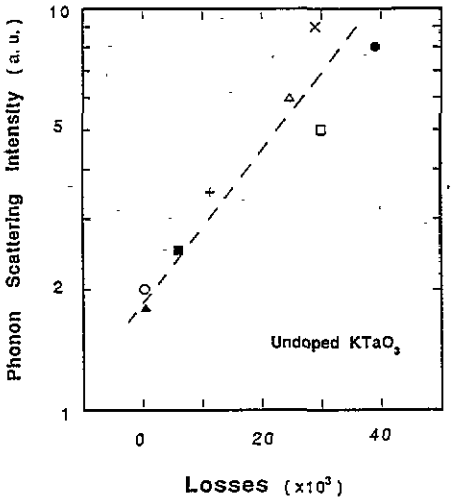

Figure 7. Phonon scattering intensity as a function of the loss intensity of eight undoped samples of $KTaO_3$: (▲) UP–(a), (○) UP–(b), (■) UP–(3), (+) P–(G), (△) P–(S), (□) P–(R), (×) P–(88), (●) P–(B). The line is a guide for the eye.

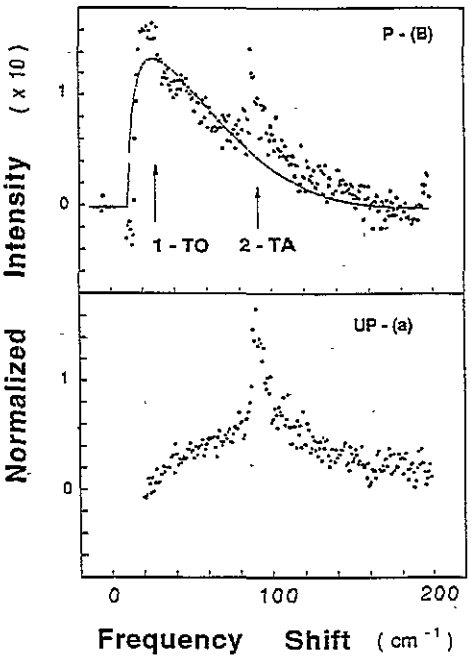

Figure 8. Comparison of the low-frequency first-order Raman line intensity for undoped samples P–(B) and UP–(a) (from work carried out by Uwe and Soneda).

samples, I_L(Nb) is smaller than in nominally pure $KTaO_3$). This result clearly indicates that the origin of the peak is not Nb, Na or Li.

To summarize, the main points stressed by the dielectric measurements are:

(i) A loss peak around $T \simeq 40$ K ($f_m \simeq 1$ kHz) exists in all the $KTaO_3$-based crystals, which is correlated with the 'additional' phonon scattering.

(ii) It seems clear that polar impurities are not candidates to explain the strong 'additional' phonon scattering in nominally pure samples.

3.3. Comparison with optical studies

Raman spectroscopy was extensively used in studying $KTaO_3$, particularly to measure the temperature variation of the soft mode. As $KTaO_3$ remains cubic down to the lowest temperature, each atomic site has a centre of inversion and first-order transitions are forbidden. However, it has been previously reported [3, 5, 31] that several one-phonon features were detected in nominally pure crystals. This means that disorder exists, leading to a breakdown of the local symmetry.

Uwe et al [5], from the temperature dependence of the Raman spectra, assigned the first-order lines to the scattering of light by what is commonly called the 'ferroelectric microregions' (FMR) [9]: in a highly polarizable material a defect can induce a local distortion that extends over a distance $r_c \simeq 1/\omega_{TO}$. As a result r_c increases as the temperature goes down, finally spanning approximately one dozen interatomic spacings at 1 K in the case of $KTaO_3$. What the origin of FMR is cannot be deduced from the observations, and it

was concluded that their properties may be characteristic of the lattice and independent of the mechanism that nucleates them. Regarding the study by Chase *et al* [3], it was deduced that niobium was not a major contributor to the breaking of lattice symmetry.

It was a key point that Uwe and Soneda were able to perform Raman experiments on two crystals supplied by us (P–(B) and UP–(a)). The results recorded at 2 K are plotted in figure 8 after the standard second-order spectrum has been subtracted. Disregarding the weak remaining part coming from the two TA phonons, only the low-frequency first-order TO_1 line is evident. It can be seen that P–(B) exhibits a pronounced one-phonon scattering, which does not appear in UP–(a). This stresses the idea that there is less disorder in the UP sample than in the P one.

During the course of the present work, Vogt [9] has made a comparison between low-temperature Raman and hyper-Raman spectra of six single crystals of $KTaO_3$ grown as pure 'according to the present state of the art by TSSG and SN techniques', in order to investigate more deeply the defect-induced microregions. One of the specimens under investigation was UP–(1) (number 3 in Vogt's paper). From this study, it was confirmed that UP–(1) exhibits a very low first-order Raman intensity and consequently a low amount of disorder.

From these observations and to summarize the experimental section, we want to stress two points:

(i) The 'additional' phonon scattering at T_m in nominally pure $KTaO_3$ is enhanced in specimens displaying strong first-order Raman scattering and a large loss peak in the dielectric susceptibility. We conclude that these three features originate from the same source, namely the distorted microregions.

(ii) As the temperature T_m is moved by introducing niobium or by applying an electric field, the additional scattering observed in thermal transport can be assigned to an interaction between acoustic phonons and the soft TO_1 mode, mediated by the distorted microregions.

It must be pointed out that thermal conductivity is extremely sensitive to small amounts of defects strongly coupled to phonons [18], so that it is not surprising to observe a drastic decrease of $K(T)$ even in what we call the 'ultra-pure' UP samples.

4. Origin of the disorder

In this section, we want to discuss possible origins of the symmetry-breaking defects responsible for microregions, among the various suggestions put forward to account for the experimental observations.

4.1. Intrinsic disorder

From NMR experiments [7], it was observed that, even in the cubic phase, the Ta^{5+} ions could sit in a local non-cubic environment on a timescale $t > 10^{-7}$ s below $T < 40$ K, allowing for symmetry breaking in $KTaO_3$ crystals. This process must involve all the tantalum ions. In this case, there is no clear reason why the experimental observations (Raman, $K(T)$, loss peak) depend strongly on the sample under study. Moreover, recent investigations performed by measuring hyper-Raman scattering unambiguously demonstrated that the distorted microregions cannot arise from quasi-static intrinsic odd-parity excitations, like hopping motions between off-centre positions of the Ta ions [9]. So, we rule out the possibility of intrinsic disorder being the origin of microregions and focus our attention on extrinsic defects.

4.2. Defect-induced disorder

No matter how much care is taken in growing samples, it is rather improbable to get nearly 'perfect' single crystals: lattice disturbances, off-stoichiometric composition, pollution leading to traces of unavoidable impurities, all are current sources of defects.

It has been stressed in previous sections that Raman scattering was unable to identify the origin of the microscopic distorted regions. However, comparison between 'nominally pure' samples and Nb-doped $KTaO_3$ suggested that niobium should not be the relevant symmetry-breaking defect. Infrared transmission experiments have been used to probe the local crystalline properties in both pure and Nb-doped specimens, and it was concluded that an excess of carbonate CO_3^{2-} radicals could be the active impurity [32]. More recently, near-infrared fluorescence experiments were performed on the same crystals and, in addition, on specimens doped with non-polar impurities (Ag, Cu, Co, etc). A characteristic luminescent impurity, universally present in both pure and doped $KTaO_3$, was detected. It was suggested that such an impurity could be formed by a complex involving the Ta^{3+} ions located near an oxygen vacancy [8]. This assignment was supported by experiments carried out on heat-treated samples (oxidized or reduced, in order to vary the number of oxygen vacancies) [33].

After recalling these previous results, our purpose is to make explicit what it is possible to extract from our own experiments.

From thermal conductivity, we confirm the presence of induced disorder whatever the type of sample. More interesting are the data gained from the dielectric susceptibility experiments. First, we are dealing with a dielectric active defect. Secondly, the unavoidable presence of the defect is confirmed as the loss peak is displayed in all the crystals investigated. Thirdly, polar impurities can be rejected as the source of microregions, as the strength of the loss peak does not correlate with the nominal concentrations.

In order to characterize this defect, we have measured $\tan\delta$ in the frequency range 10 Hz to 100 kHz for sample UP–(3). As the frequencies varied, both the magnitude and the temperature T_p of the maximum change. In figure 9 we have plotted the logarithm of frequency $\ln(f)$ versus the inverse temperature for the peak in ϵ''. The straight line means that we are dealing with an Arrhenius-type thermally activated process: $f = f_0 \exp(-E_0/k_B T_p)$. A good fit is obtained with the activation energy $E_0 = 440$ K and $f_0 \simeq 10^{11}$ Hz at $T_p \simeq 1$ mK, which stresses the point-like character of the defect. In the insert of figure 9 we have reported the variation of $\tan\delta$ against the frequency at $T = C^{te}$. The data can be satisfactorily fitted by using a Debye-type relaxation without introducing a distribution of relaxation times. This means that concentration of electric dipoles is small enough to preclude any interaction between them.

4.3. Nature of the defect

Since a polarization cluster exhibits a radius of about five atomic distances, it can be expected that the specific defect structure at the core of the microregion will be screened and that the response of the $KTaO_3$ lattice to a point defect is rather general. Then different defects could be simultaneously operative [9]. However, it is of paramount importance to try to elucidate what the major features are in order to improve the quality of the samples, and this section is devoted to giving new experimental information about the possible nature of the defect.

In light of the 'universality' of its presence, it is suggested that the most probable origin should be connected with the off-stoichiometric concentration of one of the basic elements of $KTaO_3$. In this case, oxygen vacancies could be a reasonable candidate. On the other

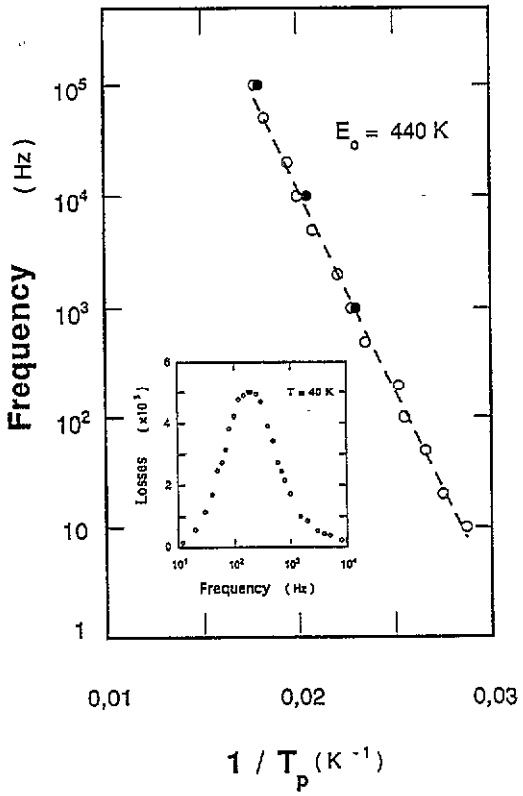

Figure 9. Arrhenius plot showing the temperature dependence of the relaxation frequency of one undoped $KTaO_3$: (○) UP–(3); and one Fe-doped specimen: (●) Fe–(B2). Insert: losses versus $\log_{10} f$ measured at 40 K of the undoped UP–(3) sample.

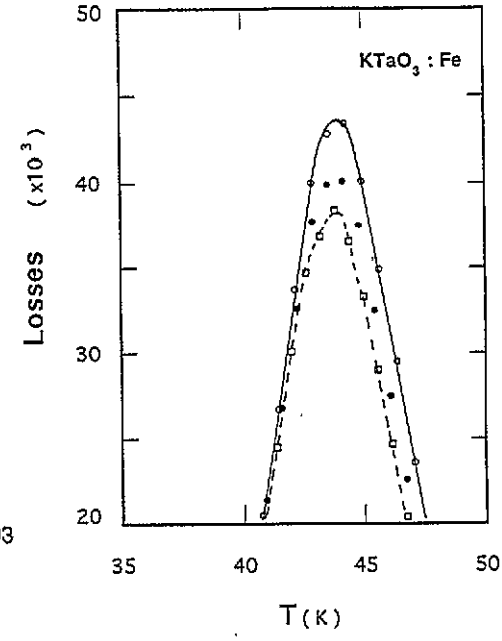

Figure 10. Dielectric losses around 40 K (f_m = 1 kHz) of Fe–(B2) after oxygen annealing: (○) as-received, (●) 100 h annealing, (□) 200 h annealing. The curves are guides for the eye.

hand, dielectric measurements performed on various compounds have evidenced that the highest loss peaks appear in Fe-doped $KTaO_3$. In this case, the observed frequency versus temperature dependence leads to an activation energy comparable with the one measured on the ultra-pure crystal UP–(3) (figure 9). It can be concluded that the same defect acts in both compounds and that iron ions could be involved in nucleating microregions.

In order to check the role of oxygen vacancies, we have annealed one Fe-doped $KTaO_3$ at 1100 °C in an oxygen (1 bar) atmosphere for two periods of 100 h. After each annealing, we observed a $\simeq$ 10% decrease in the height of the maximum in $\tan\delta$ (figure 10). These variations are significant, as the dielectric measurement reproducibility is better than 10^{-3}. However, introducing oxygen in such dense crystals is not easy: long annealings seem required, but the best experimental conditions are still unknown. To improve the efficiency of the heat treatments, it seems necessary to define the cooling-down conditions in order to keep the oxygen inside the sample. Nevertheless, these preliminary results confirm the major role of oxygen vacancies.

Finally, EPR experiments were initiated to look for both the presence and the situation of iron ions inside the samples.

It is well known that iron ions in potassium tantalate are found to be in the Fe^{3+}

state. Fe^{3+} substitutes for both Ta^{5+} and K^+. Depending on neighbourhood, two types of cubic centres (without nearby charge compensation) and two types of axial centres (Fe^{3+}–oxygen vacancy at the Ta^{5+} site or Fe^{3+}–interstitial at the K^+ site) are observed [34, 35]. Moreover, a low-symmetry rhombic Fe^{3+} centre was evidenced and more recently deeply investigated [36]. The main characteristic of the rhombic crystal field results in an EPR line with $g_{eff} = 4.27$ for $H \| \langle 100 \rangle$.

Experiments performed on different types of crystals gave a new insight into the physics of microregions:

(i) All the EPR spectra recorded at room temperature on UP, P and Fe-doped samples exhibit the lines attributed to cubic and axial Fe^{3+} ions (figure 11). The arrows indicate the positions of lines due to Fe^{3+} ions sited in cubic symmetry. Moreover, part of the central line comes from axial Fe^{3+} [30]. It should be noted that, at equivalent incident power, the amplification rate is 10^4 times larger in the case of P and UP samples, showing that the amount of Fe^{3+} ions is very small, although detectable, in undoped crystals. This clearly means that, even in the purest available specimens, iron appears as an unavoidable impurity.

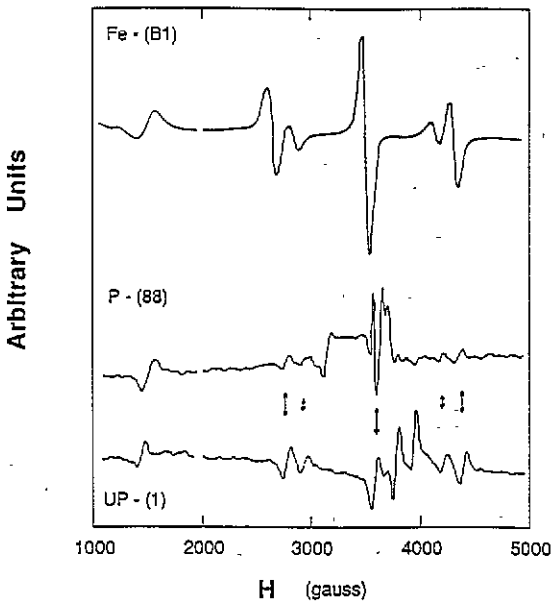

Figure 11. Examples of EPR spectra recorded on Fe-doped, P and UP samples ($T = 300$ K, $f = 9$ GHz, $H \| \langle 100 \rangle$). Around 1600 G, we note the presence of the $g_{eff} = 4.27$ line (the amplification rate is 10 times larger in P and UP data).

(ii) By irradiation with electrons, the cubic to axial Fe^{3+} ratio is observed to change in the Fe-doped sample: simultaneously the central line at $g = 2$ increases and the cubic contribution decreases. But we failed to observe any change in the magnitude of the loss peak at 42 K, indicating that no correlation exists between the number of axial Fe^{3+} ions and the dielectric peak. This suggests that this defect is not at the origin of the microregions.

(iii) In the same samples, the $g_{eff} = 4.27$ line is observed. Now, the magnitude of this line scales with the height of the loss peak: it appears to be very small, although unambiguously detectable, in UP samples and more important in Fe-doped $KTaO_3$ (figure 11). In the Fe-doped sample, the width must be due to interactions between iron ions, as the concentration is 1%. It must be noted that this line was also observed in P–(R). This result is of paramount importance: very low concentrations of rhombic iron could be at the origin of the local distortions, although in any case the main part of Fe^{3+} sits in cubic or axial symmetry.

In their recent paper, Pechenyi *et al* [36] performed a detailed study of rhombic Fe^{3+} in $KTaO_3$. They note that heat treatment in an oxidizing atmosphere leads to the reduction of rhombic lines: this is consistent with the decrease in $\tan\delta$ we observe in our oxygen annealed sample. From experimental data and theoretical considerations they conclude that rhombic iron should be generated by a Fe^{3+} in a Ta^{5+} site with a positive interstitial compensation in ⟨110⟩ direction. This model is compatible with our data, although the presence of a complex defect cannot be discarded (as an example, Fe^{3+} at the K^+ site with a vacancy in the oxygen octahedra also induces a ⟨110⟩ rhombic distortion). In this case, the additional charge compensation should be located further, leading to a more extended defect. In any case, oxygen vacancies associated with iron ions unambiguously seem to be at the origin of microdistorted regions in potassium tantalate.

5. Macroscopic properties of the 'purest' available $KTaO_3$

Taking into account the results carried out by different groups, it seems suitable to define the main features that an undoped crystal should offer in order to be considered as a 'pure' sample:

(i) absence of first-order Raman lines;
(ii) absence of loss peak at 42 K in dielectric permittivity;
(iii) absence of minimum in thermal conductivity; and
(iv) absence of $g_{\text{eff}} = 4.27$ line in EPR experiments.

In the currently available samples, none of these conditions are fulfilled. It is then worth while to assume that the purest specimens exhibit the smallest features. It follows that the UP labelled samples look like the best presently available samples.

As a matter of reference, we add in this publication some macroscopic properties, all measured on the same large-size crystal, namely UP–(2).

We recall that the thermal conductivity for this specimen is shown in figure 3. In figure 12 we have plotted the specific heat between 1 and 20 K in a C_p/T^3 versus T^2 graph. Both shape and magnitude are very similar to the results previously obtained on a different sample [37]. At low temperature, C_p tends to a T^3 behaviour, which is expected for an insulating material from the Debye theory. Moreover, the measured limit value $C_D = 20$ J mol^{-1} K^{-1} is in a rather good agreement with the value calculated by using the elastic constants. Data are compared with a model given by Migoni *et al* [38], which was used to analyse a comprehensive set of phonon dispersion curves [24] taking into account the temperature dependence of the low-frequency modes. It can be seen that the general shape is obtained and a reasonable quantitative agreement is achieved below 5 K. As a matter of comparison, a 3% Nb-doped $KTaO_3$ was measured. Above 3 K the data are quite similar to those of the undoped sample. The origin of the C_p increase below 3 K is not understood. These results differ markedly from those by Lawless [15], and demonstrate that a small amount of polar impurities does not change the specific heat of $KTaO_3$ above 3 K in a noticeable way.

Finally, we report in figure 13 both the real and imaginary parts of the dielectric susceptibility at low temperature on a semi-logarithmic plot. The classical increase of ϵ' as the temperature goes down is observed. Below 2 K, a saturation value (4100) is reached, which remains perfectly constant down to 80 mK, the lowest available temperature.

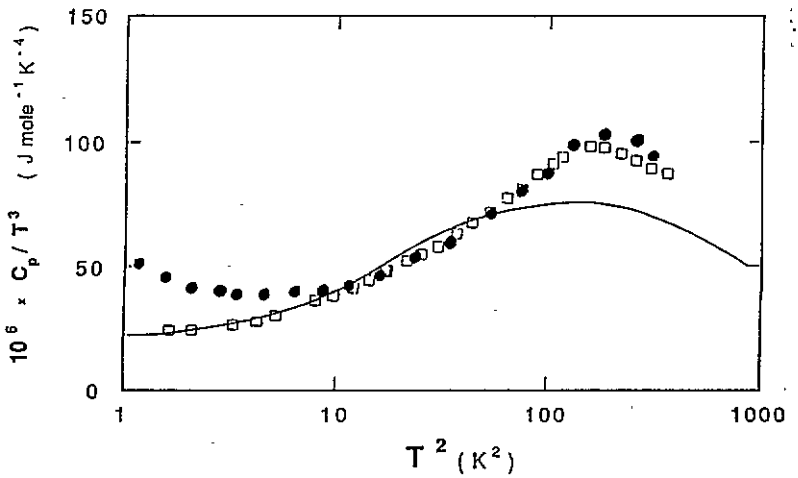

Figure 12. Specific heat of one nominally pure ((□) UP–(2)) and one Nb-doped ((●) 3% Nb) $KTaO_3$. The specific heat calculated by Migoni [24, 38] is shown as a full curve.

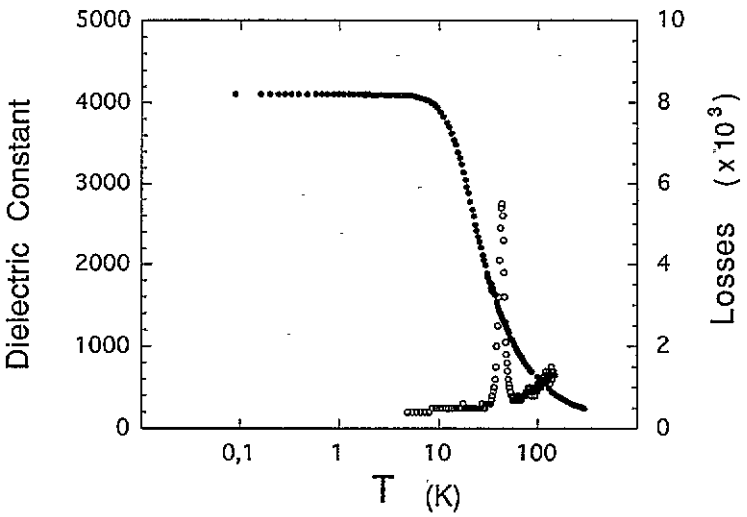

Figure 13. Dielectric constant (f_m = 1 kHz) of the ultra-pure sample UP–(2) showing the saturation of the real part (●) at low temperature simultaneously with the loss peak (○).

6. Summary

In this paper, we support the idea that disorder in nominally pure $KTaO_3$ is of extrinsic nature. We think that its origin is from extended defects located around rhombic Fe^{3+} ions associated with oxygen vacancies. Owing to the high polarizability of the lattice, these defects seem able to drive an interaction between the acoustic phonons and the soft optic mode ω_{TO} and should be responsible for the dip around 8 K observed in the thermal conductivity of undoped $KTaO_3$. Additionally, they should account for the dielectric dissipation observed and the presence of the $g_{eff} = 4.27$ line in EPR experiments. At

the present time, these defects look unavoidable in growing nominally pure $KTaO_3$ single crystals.

Acknowledgments

The authors wish to thank B Daudin, M Fontana, M Maglione and R Cox for fruitful discussions in the course of this work, N Bernhoeft for a critical reading of the manuscript, and D Arnaud, J A Favre and R Picard for technical assistance. Thanks are due to S Jandl, D Rytz, H Uwe and H Vogt for providing samples and performing additional experiments.

References

[1] Granicher H and Muller K A 1971 *Mater. Res. Bull.* **6** 977
[2] Hochli U T, Weibel H E and Boatner L A 1977 *Phys. Rev. Lett.* **39** 1158–61
[3] Prater R L, Chase L L and Boatner L A 1981 *Phys. Rev.* B **23** 221–31
[4] Hochli U T, Knorr K and Loidl A 1990 *Adv. Phys.* **39** 405–615
[5] Uwe H, Lyons K B, Carter H L and Fleury P A 1986 *Phys. Rev.* B **33** 6436–40
[6] Toulouse J, Di Antonio P, Vugmeister B E, Wang X M and Knauss L A 1992 *Phys. Rev. Lett.* **68** 232
[7] Rod S, Borsa F and van der Klink J J 1988 *Phys. Rev.* B **38** 2267–72
[8] Grenier P, Bernier G, Jandl S, Salce B and Boatner L A 1989 *J. Phys.: Condens. Matter* **1** 2515–20
[9] Vogt H 1991 *J. Phys.: Condens. Matter* **3** 3697–709
[10] Steigmeier E F 1968 *Phys. Rev.* **168** 523–30
[11] Salce B, de Goer A M and Boatner L A 1981 *J. Physique Coll.* **42** 424
[12] Salce B and Boatner L A 1986 *Proc. 5th Int. Conf. on Phonon Scattering in Condensed Matter (Urbana, IL) Springer Ser. Solid State Sci. 68* ed A C Anderson and J P Wolfe (Berlin: Springer) pp 272–4
[13] Salce B and Boatner L A 1988 *Ferroelectrics* **79** 249–52
[14] Lawless W N 1976 *Phys. Rev.* B **14** 134–43
[15] Lawless W N, Rytz D and Hochli U T 1981 *Ferroelectrics* **38** 809–12
[16] Hannon D M 1967 *Phys. Rev.* **164** 366–71
[17] de Goer A M 1969 *J. Physique* **30** 389–400
[18] Salce B and de Goer A M 1979 *J. Phys. C: Solid State Phys.* **12** 2081–101
[19] Challis L J and de Goer A M 1984 *The Dynamical Jahn-Teller Effect in Localized Systems* ed Y E Perlin and M Wagner (Amsterdam: Elsevier) ch 12, pp 533–708
[20] Fleury P A and Worlock J M 1967 *Phys. Rev. Lett.* **18** 665–7
[21] Shirane G, Nathans R and Minkiewicz V J 1967 *Phys. Rev.* **157** 396–9
[22] Fontana M D, Bouziane E and Kugel G E 1990 *J. Phys.: Condens. Matter* **2** 8681–9
[23] Axe J D, Harada J and Shirane G 1970 *Phys. Rev.* B **1** 1227–34
[24] Perry C H, Currat R, Buhay H, Migoni R M, Stirling W G and Axe J D 1989 *Phys. Rev.* B **39** 8666–76
[25] Prater R L, Chase L L and Boatner L A 1981 *Phys. Rev.* B **23** 5904–15
[26] Kamitakahara W A, Loong C K, Ostrowski G E and Boatner L A 1987 *Phys. Rev.* B **35** 223–7
[27] Fleury P A and Worlock J M 1968 *Phys. Rev.* **174** 613–23
[28] Fujii Y and Sakudo T 1976 *J. Phys. Soc. Japan* **41** 888–93
[29] Rytz D, Chatelain A and Hochli U T 1983 *Phys. Rev.* B **27** 6830–40
[30] Gravil J L 1991 *Doctorat* UJF Grenoble (France)
[31] Yacobi Y 1977 *Int. Conf. on Lattice Dynamics (Paris)* pp 453–6
[32] Houde D and Jandl S 1986 *Solid State Commun.* **60** 45–8
[33] Jandl S, Banville M, Dufour P, Coulombe S and Boatner L A 1991 *Phys. Rev.* B **43** 7555–60
[34] Rytz D, Hochli U T, Muller K A, Berlinger W and Boatner L A 1982 *J. Phys. C: Solid State Phys.* **15** 3371–9
[35] Bykov J P, Glinchuk M D, Karmazin A A and Laguta V V 1983 *Sov. Phys.–Solid State* **25** 2063–5
[36] Pechenyi A P, Glinchuk M D, Antimirova T V and Kleemann W 1992 *Phys. Status Solidi* b **174** 325–33
[37] Salce B, Calemczuk R, Bonjour E, Migoni R and Boatner L A 1986 *Proc. 2nd Int. Conf. on Phonon Physics (Budapest)* ed J Kollar *et al* (Singapore: World Scientific) pp 979–81
[38] Migoni R, Bilz H and Bauerle D 1976 *Phys. Rev. Lett.* **37** 1155–8